

Integrated Numerical and Experimental Investigations of the Active/Passive Aeroelastic Concepts on the European Research Aeroelastic Model EuRAM

(Received: June 8, 2010. Revised: July 6, 2010. Accepted: July 15, 2011)

S. KUZMINA¹
F. ISHMURATOV²
M. ZICHENKOV³
V. CHEDIK⁴

Abstract

The European Research Aeroelastic Model (EuRAM) was developed as an experimental platform for the demonstration of the new technical approaches and concepts arising from the goals of the European 3AS (Active Aeroelastic Aircraft Structures) FP5 Project. The EuRAM demonstrator was designed and fabricated to test three concepts: Aeroelastic Wing Tip Controls, All-Movable Vertical Tail and Selectively Deformable Structures. Finite Element and aeroelastic models of the complete EuRAM airplane were created for prediction of the strength and aeroelastic behaviour, multidisciplinary optimization and updating following the wind tunnel tests. The complete EuRAM was tested in TsAGI's T-104 wind tunnel. Components of the EuRAM (semi-wings with ordinary and new control surfaces, ordinary and all-movable vertical tails) were tested separately in different wind tunnels by partners of the 3AS Project. A wide range of multifunctional possibilities and reliability of the EuRAM model have been demonstrated. The analysis and tests of the EuRAM model proved its ability to delay divergence and flutter onset, and also to withstand large gust loads, so allowing for a test campaign without high risk of model damage or failure. Results of the two-level approach for structural optimization of the EuRAM wing under stress and aeroelastic constraints are presented. It was demonstrated that the constraints on aileron effectiveness play a significant role in design of the wing structure, requiring extra weight to be added to compensate for the aeroelastic requirements. It was also shown that using of non-traditional wing tip ailerons reduces this weight increase.

1. Introduction

The European Research Aeroelastic Model (EuRAM) was developed as an experimental platform for the demonstration of the new technical approaches and concepts developed as part of the European 3AS (Active Aeroelastic Aircraft Structures) FP5 Project [1, 2, 3]. 3AS aimed to improve the flight performance, economy and efficiency of aircraft through the development of active and passive aeroelastic concepts. These concepts allow considerable reduction in aerodynamic drag, structural weight and operating costs. The EuRAM demonstrator, a four-engine wide body transport aeroelastic wind tunnel model of 1:10 length scale, span=5.7m and mass=200kg, was designed and fabricated to test three specific concepts:

- Aeroelastic Wing Tip Controls (AWTC) - new control surfaces at the wing tip, forward of the elastic axis, to adjust the flexible wing deformation to the optimum shape for minimum induced drag
- All-Movable Vertical Tail (AMVT) - replacement of the existing vertical tail by a smaller, all-movable surface with variable rotational attachment stiffness. The rotational axis is located behind the elastic axis, and the torsional stiffness can be adjusted to the flight condition

¹ Deputy Head of Division, Aeroelasticity Department, TsAGI, Moscow

² Head of Division, Aeroelasticity Department, TsAGI, Moscow

³ Deputy General Director, TsAGI, Moscow

⁴ Head of Division, Static and Heat Strength Department, TsAGI, Moscow



Figure 1: The complete EuRAM in TsAGI wind tunnel T-104.

- Selectively Deformable Structures (SDS) - modification of the inner aileron using a new kind of structure that allows large deformations with small internal forces, thereby creating a more continuous deformed shape

The complete model was tested in TsAGI's T-103 and T-104 wind tunnels (Fig. 1). Components of the EuRAM (semi-wings with ordinary and new control surfaces, ordinary and all-movable vertical tails) were tested separately in different wind tunnels by partners of the 3AS Project [4, 5]. Finite Element (FE) models of the complete EuRAM airplane were created for multidisciplinary optimization and analysis. In addition to the FE models (in NASTRAN format) the TsAGI software ARGON [6] was used for computing strength, static and dynamic aeroelasticity, and aeroservoelasticity characteristics. The ARGON code was used to both predict the results and also to update analytical models. Updating the mathematical models of the elastic structure was carried out at different stages on the basis of stiffness measurements, the Ground Vibration Test (GVT) and wind tunnel tests. Such an integrated approach allows validity of the results to be provided.

2. Design, manufacture and wind tunnel testing of the EuRAM

2.1 Requirements for the EuRAM and experimental facilities

The following main requirements for the demonstrator and testing were formulated according the 3AS project goals:

- modular structure with the possibility of semi-wings and vertical tails being separately tested in different wind tunnels
- large scale and compartment-beam structure with easy changing of different configurations and control surfaces
- using actuators for ailerons and nontraditional surfaces dynamic control
- several different attachment types incorporated in the fuselage for adjusting the AMVT rotational stiffness and also basic vertical tail with rudder
- wind tunnel tests of the complete model on a balance and under "free-free" conditions
- measurement of static aeroelasticity, flutter and aeroservoelastic characteristics for complete model and also separate components.

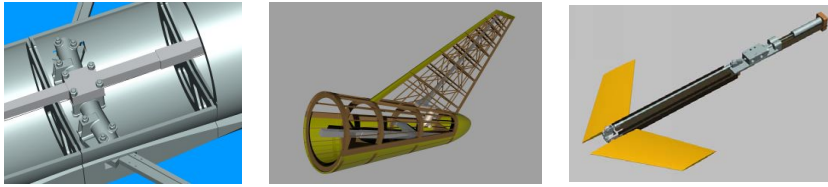


Figure 2: Fuselage central part (left), vertical tail structure (middle) and forward aileron (right).

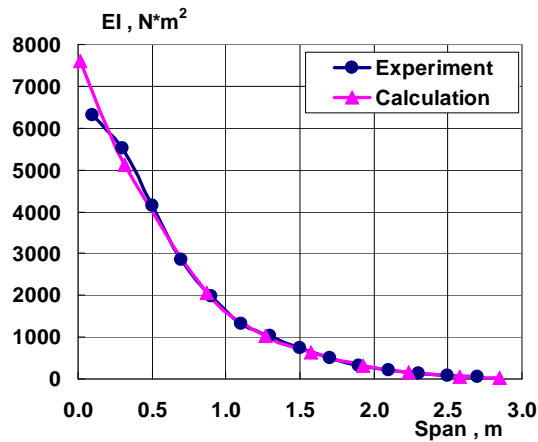


Figure 3: Comparison between experimental and computed wing stiffness.

2.2 Model design and manufacture

The T-flex 3-D CAD system was used for the design of new components of the model and preparation of the necessary drawings. As examples, the central parts of the fuselage, the tail structure and the forward aileron with pylon and integrated actuator/sensor are shown in Fig. 2.

New control surfaces were employed that gain a positive effect from the wing elastic deformation [7]. The EuRAM fuselage, wings and tails were constructed using aluminum beams with rectangular and H-shape cross-sections. Plywood was used as a main material for the compartment structures. The forward aileron and pylon were of a carbon/fiber/plywood structure.

2.3 Laboratory tests

Laboratory measurements of stiffness, mass and modal characteristics of the EuRAM components, and a ground vibration test of the complete model configurations, were carried out. The qualification of the model parameters and preparation data for creation of adequate mathematical models and their corrections was performed. An example of the correlation between experimental and theoretical wing beam stiffness along the span is illustrated in Fig. 3.

The ground vibration test of the complete EuRAM was conducted in the frequency range from 1Hz to 10Hz. Natural symmetric/asymmetric elastic modes for five structural configurations were identified inside this frequency range. Figure 4 shows the first wing bending asymmetrical mode for the EuRAM configuration with forward tip aileron. All the natural frequencies of the control surfaces were above 20Hz.

2.4 Wind Tunnel Tests

Wind tunnels (WT) tests have been performed on different EuRAM components: AMVT, left semi-wing, forward aileron and inner aileron with SDS, as shown in Figs. 5 and 6.

For the static aeroelasticity characteristics measurement of the complete EuRAM, the model was attached to a vertical strut with 6-components strain-gage balance at the model's centre of gravity (Fig. 7, left). The model suspension

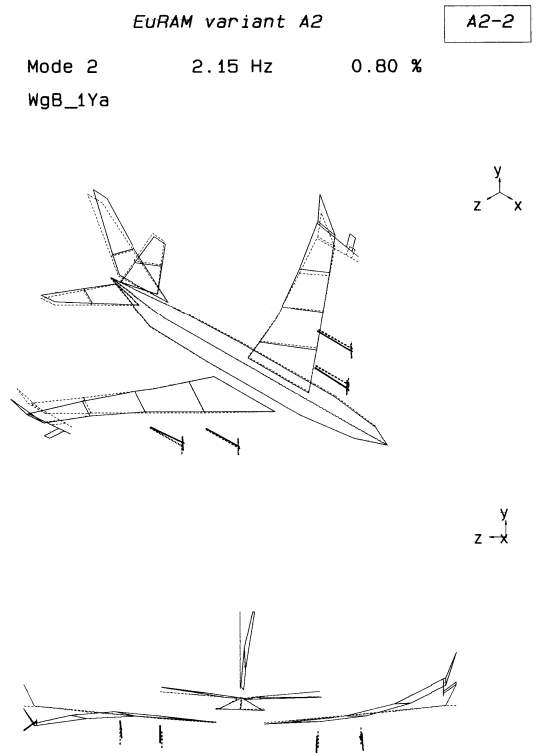


Figure 4: Experimental first wing bending asymmetrical mode.

Figure 5: AMVT model (left) and static deformation of half-wing (right).



Figure 6: Forward aileron (left) and inner aileron with flexible SDS (right).





Figure 7: Static aeroelasticity test (left) and flutter test on the complete EuRAM (right) in WT T-104.

system enabled the angle of attack and sideslip angle to be changed. Deflection angles of ailerons, tip and under wing forward ailerons, basic rudder and all-movable vertical tail could also be mechanically changed and fixed.

For the flutter tests in the T-104 tunnel, the complete EuRAM was supported by a universal "two points" cable low frequency suspension system designed in TsAGI especially for the investigation of dynamically scaled model flutter characteristics (Fig. 7, right). The suspension system provides five degrees of freedom for the model as a rigid body within a frequency range up to 1Hz. Choosing such suspension system structural parameters and geometry provides enough static and dynamic stability of the model so that it behaves as a rigid body for all configurations. Signals of strain gauges and accelerometers, as well as video and visual information, were used for the analysis of the model flutter characteristics. The analysis of measured data showed that necessary flutter margins are ensured for all test configurations of the EuRAM. Flutter characteristics of the model with the new wing tip surfaces attached somewhat degraded for speed more than 34m/s; however, adequate safety margins were still maintained.

For the purposes of aeroservoelasticity investigations, the complete EuRAM was installed in the T-104 wind tunnel on the same cable low frequency "two points" suspension system as used for the flutter tests. The model was equipped with miniature hydraulic actuators with maximum force of about 300N. "Sensorex" inductive type displacement sensors with amplifiers were used both in the actuator feedback loop and for measurement of the actuator rod displacements, ensuring adequate deflection of both ordinary and forward ailerons. A special analog unit provided the necessary feedback loop for the ailerons' actuator. Two PCs with analog-digital and digital-analog transfer blocks provided the acquisition and control of sensor signals, excitation signals and control law digital filter for the closed loop experiments. The sampled frequency for the open loop case was 250Hz, 1000Hz for the closed loop. A cascade of two wings, controlled by the PC driving a hydraulic actuator, in the entrance to the test section allowed simulation a single gust of different harmonic gusts and random turbulence (Fig. 8).

Two aspects of the active aeroelasticity concept were studied:

- use of wing elasticity for increase of the roll control characteristics and decrease of the induced drag with aid of controls located forward of the wing stiffness axis;
- use of rotational elasticity of reduced size all-movable vertical tail for improvement of lateral stability and controllability.

3. Computational Models

The computational beam model was designed using the ARGON software package, leading to the manufacture of the beam-compartment Dynamically Scaled Models (DSM). The developed model was based on the method of prescribed forms (Ritz polynomial method) where the structural parts of the DSM were modeled with bending/torsion beams and concentrated masses (Fig. 9). The



Figure 8: Gust response test on on the EuRAM .

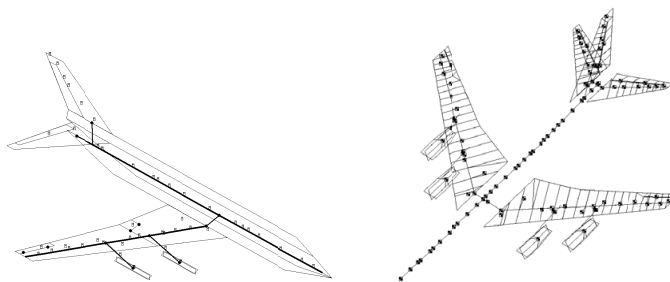


Figure 9: Computation model in ARGON (left) and FE model of EuRAM with SDM aileron.

structural parts are joined by rigid springs. The compartments of the DSM were not modeled and the deformation of the lifting surfaces was considered to be smooth.

Finite element (FE) models of structural parts and full DSM were then also developed in NASTRAN. Compartments of the lifting surfaces were modeled using rigid plate elements to aid the visualization of the displacements (Fig. 10). The displacement field for analysis of the aerodynamic forces was defined by one-dimensional splines generated on the nodal displacements of the spars. The finite element models are described in more detail in [8]. The development and refinement of the analytical models were performed in the following sequence: preliminary models of structural parts, refinement of preliminary models after design, manufacturing, modal and aeroelastic predictions, assembly of the full DSM, modal and aeroelastic predictions.

It was felt necessary to validate the effectiveness of the concepts considered in this project on a full scale computational airplane model, developed on the basis of its DSM. The geometrical sizes of the mathematical model of the full scale airplane were defined by multiplication of the DSM sizes by the length scale coefficient.

The structural layout was chosen on the basis of known structural layouts of existing wide body airplanes and from experience. The traditional approach of modelling using two-dimensional shell elements and one-dimensional beam elements was employed for the development of the full scale airplane model (Fig. 10, left). The aerodynamic model used for all structural models is shown in Fig. 10, right. Unsteady aerodynamic forces in the dynamic aeroelasticity problems were analyzed using the doublet-lattice method.

The mathematical model of the full-scale airplane has a quite reasonable lift-to-drag ratio, related to induced drag only, at cruise flight regime. Supercritical airfoils with thickness-to-chord ratio 14.4% at the wing root and 9% at the wing tip were used along with jig twist angles of 3 at the wing root and -1 at

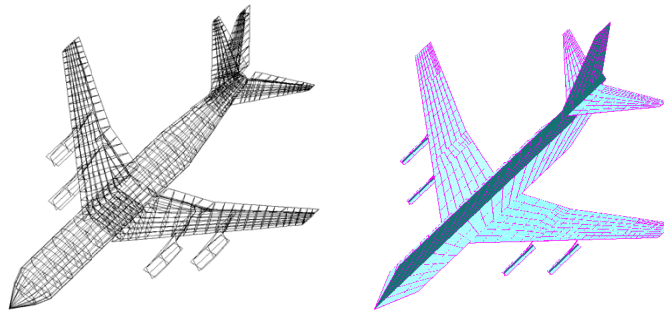


Figure 10: FE model of full scale EuRAM (left) and aerodynamic model (right).

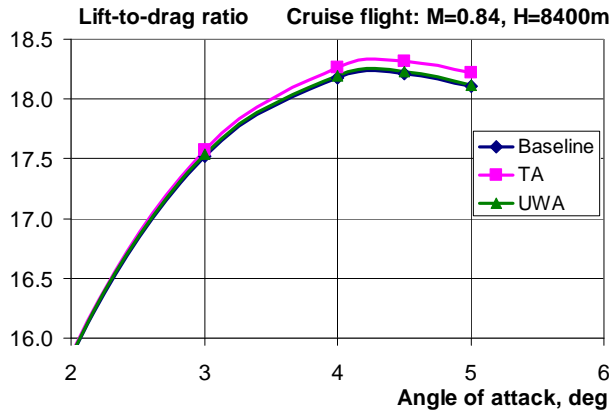


Figure 11: Comparison of lift-to-drag ratio of full aircraft for different configurations, TA-wing tip aileron, UWA-under wing aileron.

the wing tip. Figure 11 shows the comparison of lift-to-drag ratios for different configurations. The configuration with tip aileron (TA) has a slightly greater value of lift-to-drag ratio mainly due to its larger effective aspect ratio.

4. Static Aeroelastic Characteristics

Most of the considered concepts in this work that aim to use aeroelastic deflections in a positive way are mainly related to the static aeroelasticity characteristics. Therefore, considerable attention was paid to the static aeroelasticity studies. Elastic displacements and streamwise twist angles along wing spar at angle of attack $\alpha=5$ and flow speed $V=25\text{m/s}$ are shown in Figs. 12 and 13 with, and without, the structural weight included.

The wing tip displacement is 0.15 m in the upward direction, and decrease of angles of attack in the tip section is ≈ 2.4 for analysis without account of gravity forces. Accounting for structural weight reduces the wing tip displacement almost by 0.12 m. The roles of bending and torsion angles in the streamwise angle of attack are shown in Fig. 14. The large contribution of the bending

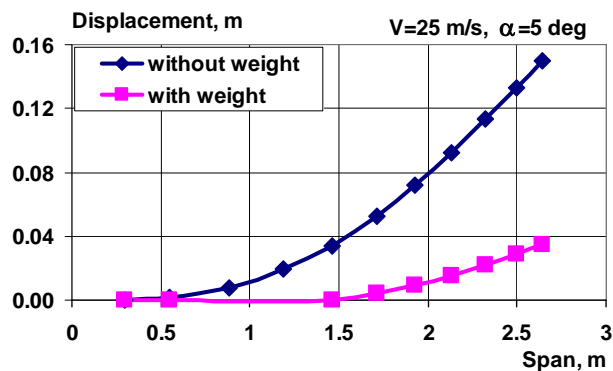


Figure 12: Elastic displacements of EURAM model.

Figure 13: Streamwise twist angles along EU-RAM wing.

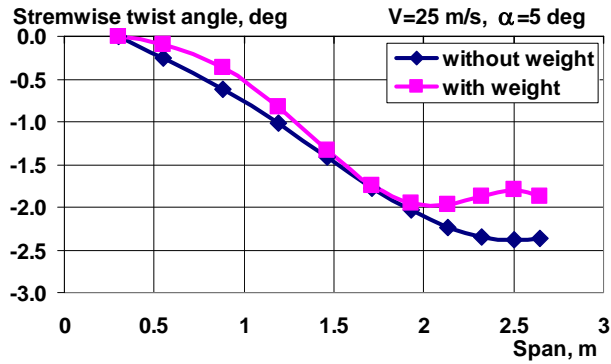
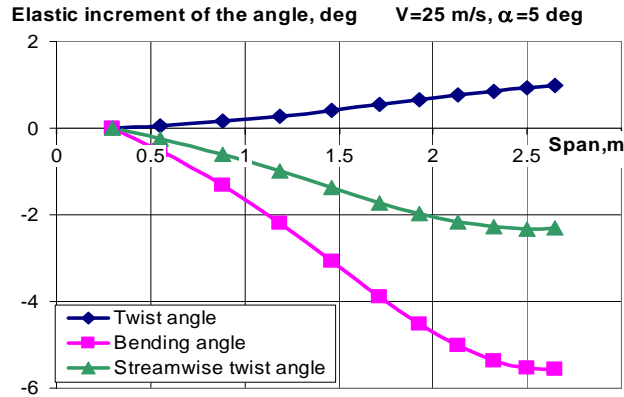


Figure 14: Contribution of bending and torsion to the streamwise angle of attack.



angle to the streamwise angle of attack can be seen.

One of the most important static aeroelastic characteristics is the effectiveness of the outer aileron. Classically, this is reduced due to aeroelastic twist, and the outer aileron achieved reversal on lift at flow speed $V=25$ m/s, and reversal on roll at flow speed $V=36$ m/s. A different interpretation of this phenomenon is presented in Fig. 15. Here the influence of flow speed and structural elasticity on distribution of aerodynamic forces is shown through consideration of a fixed root wing structure with aileron deflection of 1 degree. The shear force in the wing root achieves a maximum value at flow speeds in the range $V=15-20$ m/s, but becomes practically zero at flow speed $V=25$ m/s. The bending moment also achieves maximum value at flow speeds around $V=20$ m/s, and then decreases for further increase of the flow speed.

It is necessary to bear in mind the use of the DSM static aeroelasticity characteristics for full scale airplane that they were defined for fixed structure of DSM. Additional inertial forces are applied to real structures in free flight, and they also cause additional displacements and redistribution of aerodynamic forces.

The influence of structural elasticity on the location of airplane aerodynamic center XF for the actual airplane scale of dynamic pressures is shown in Fig. 16. The analytical and experimental results are in good agreement for fixed structure in incompressible airflow ($M=0.07$). The characteristics of free-free structures are different from fixed structure. Also, it is necessary to take into account the influence of Mach number on the full scale airplane behavior, and Fig. 16 shows that for in-cruise flight $M=0.84$ the location of aerodynamic center of the full scale airplane in free flight is significantly different from the location found in the wind tunnel tests. Note the good comparison between the analytical and experimental results.

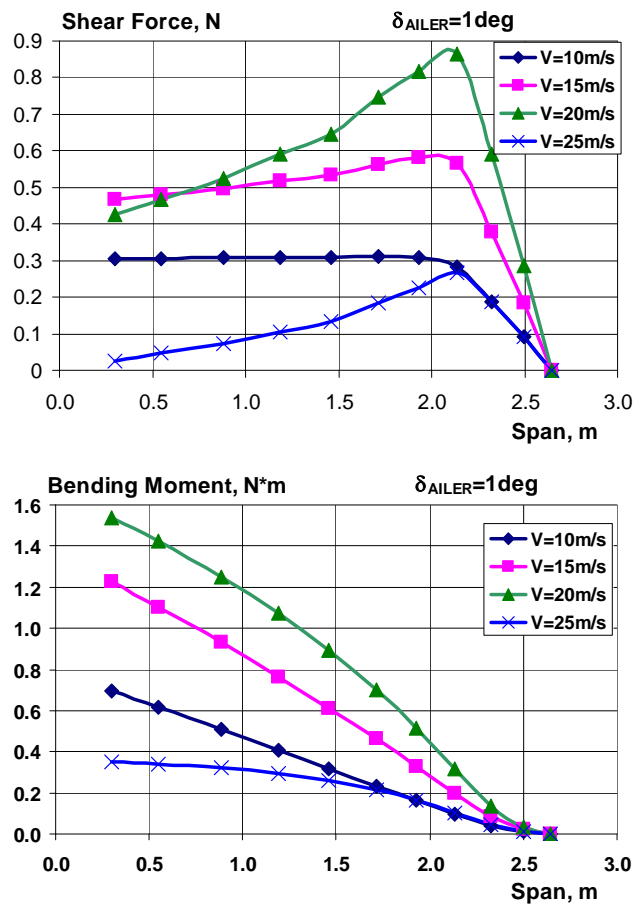


Figure 15: Shear force (top) and bending moment (bottom) along wing.

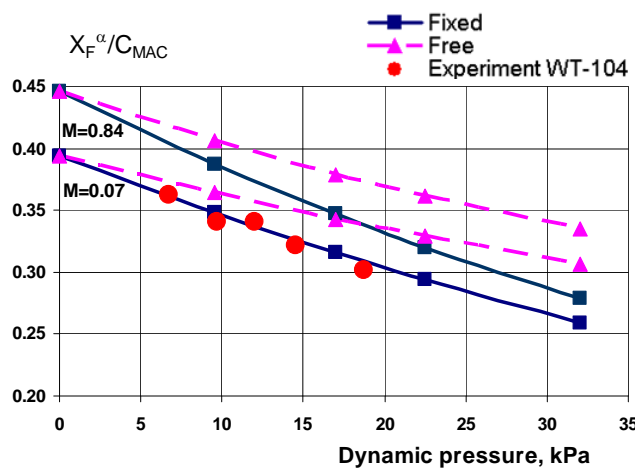
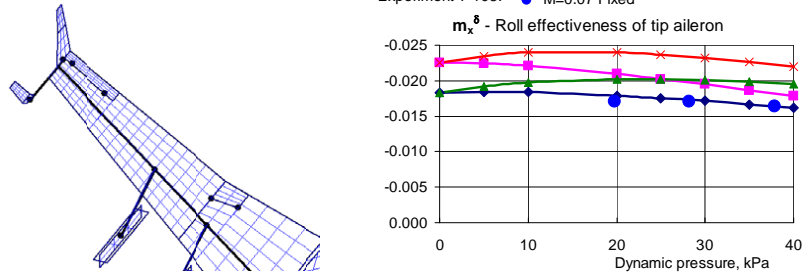


Figure 16: Influence of structural elasticity on aerodynamic center location.

Figure 17: Roll effectiveness of wing tip aileron.



5. Aeroelastic Wing Tip Controls Concept

The objective of the concept is to investigate new types of control surface that generate an active elastic deformation of the wing leading to desired aerodynamic characteristics. Figure 17 shows the comparison for the roll effectiveness m_x of the wing tip aileron. For the fixed structure the analytical results are in a good agreement with the experimental ones (recalculated for scales of the actual airplane). Unlike a regular aileron the effectiveness of the wing tip aileron is practically not decreased. On a free structure, the inertial forces arising because of roll angular acceleration twist the wing to "useful" angles. Therefore, the effectiveness of the wing tip aileron on full scale airplane increases. However, inertial forces should be taken into account for the full scale (FS) structure because the DSM is not similar to full scale airplane on mass-inertial characteristics.

5.1 Dynamic effectiveness of control surfaces

One of the key aspects of the active aeroelasticity concept is the active control system. Frequency response functions (FRF) for load factors at various structural sections, and for wing root loads, are computed to evaluate the possibilities of using of AWTC for active control system. Results of this analysis were found to be in satisfactory agreement with the experimental data. For example, a comparison of FRF for load factor at the wing tip (N_w) and wing root bending moment (M_b) due to symmetrical harmonic deflection of regular ailerons is shown in Figs 18 and 19 for airflow speed $V=22\text{m/s}$. The figures show that analysis characteristics agree well with the experimental data both on amplitude and phase. Some of the disagreement in amplitude can be explained by the well known peculiarity of linear panel aerodynamics that amplifies somewhat the lifting properties. Also, some difference in structural damping may have to be considered. It is interesting to compare the dynamic effectiveness of different wing control surfaces: regular (basic) aileron, tip aileron (TA), and aileron on a pylon under wing (UWA). Their effectiveness for the gust load alleviation system was studied in [9]. Here we consider a comparison of the aeroelastic wing tip controls (AWTC) effectiveness on wing root bending moment in frequency domain for different airflow speeds (Figs 20 and 21). The dynamic effectiveness of the basic aileron remains greater at airspeed $V=22\text{m/s}$, but at $V=30\text{m/s}$ the AWTC has a considerably higher effectiveness in the frequency range of the first natural elastic mode. The regular aileron has larger effectiveness in the frequency range of higher elastic modes.

5.2 Strength and aeroelastic structural optimization of the EuRAM wing using a two-level approach

Structural optimization was performed for the EuRAM full scale airplane with different types of aeroelastic wing tip control surfaces (AWTC). The results obtained demonstrate the influence of the AWTC on the optimum structural

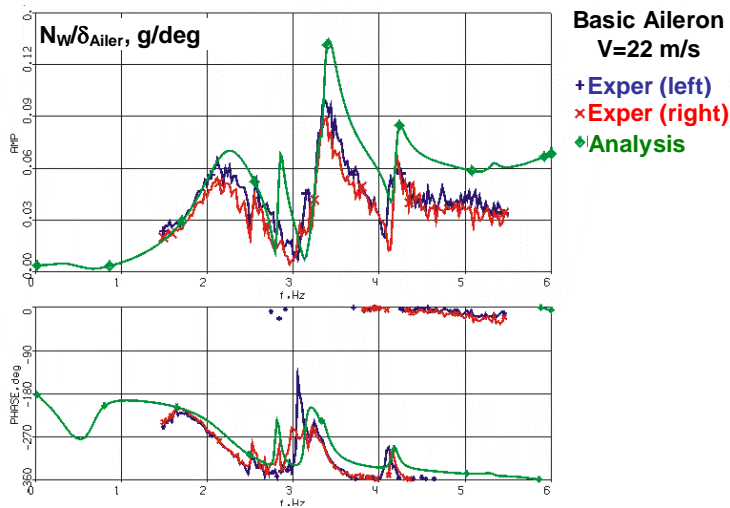


Figure 18: FRF for load factor at the wing tip due to regular aileron oscillation.

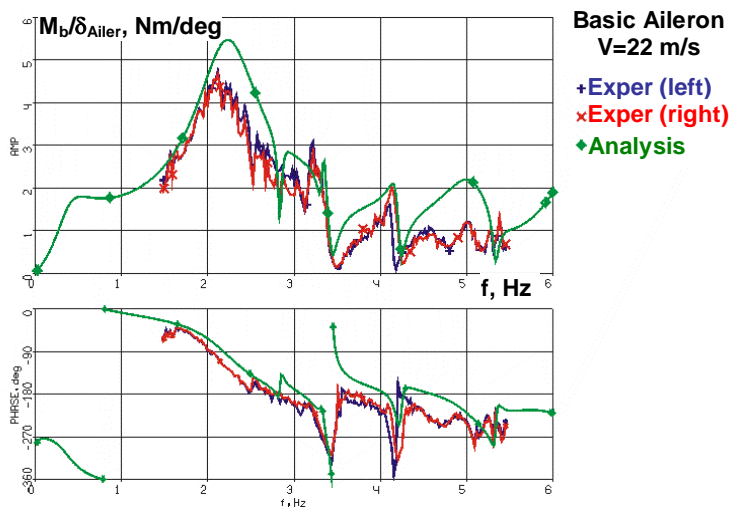


Figure 19: FRF for wing root bending moment due to regular aileron oscillation .

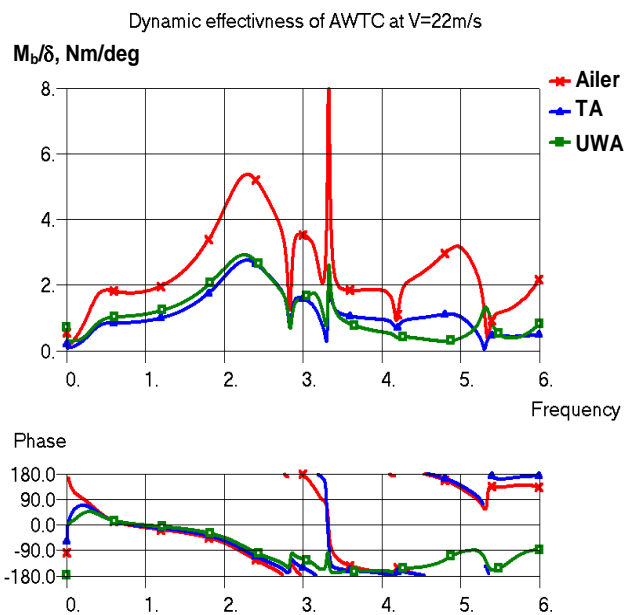


Figure 20: Dynamic effectiveness of AWTC at V=22m/s.

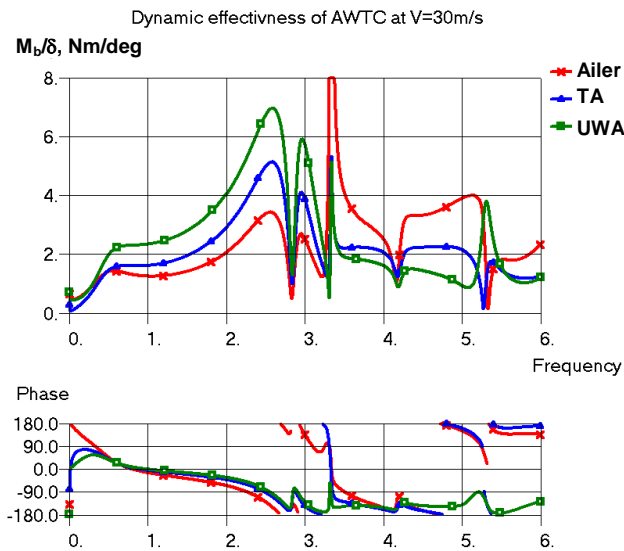


Figure 21: Dynamic effectiveness of AWTC at $V=30\text{m/s}$.

weight and aeroelastic characteristics. A comparative analysis of baseline configuration with the new "active aeroelastic" configurations was conducted. The problem of preliminary design of an aircraft structure is to define structural sizes that will ensure minimum weight while satisfying the numerous multidisciplinary constraints. These constraints are of different types for many load conditions in disciplines such as strength, static and dynamic aeroelasticity. The responses in the disciplines can be analyzed by programs which use structural models of different fidelity and different approach.

The ARGON multidisciplinary system integrates several aircraft disciplines:

- linear aerodynamics
- analysis of maneuver and dynamic loads on elastic structure
- structural analysis
- modal analysis
- static aeroelasticity
- flutter
- aeroservoelasticity

The problems of aeroelasticity and loads calculation are solved by using the discrete-continual model of prescribed forms (first level model). The finite element model (second level model) is used for detailed evaluation of stresses and displacements of structure. The design procedure based on the two-level approach is shown in Fig. 22.

The aeroelastic/strength design cycle starts with calculation of aerodynamic and inertial loads for various parameters of maneuvers. Optimization under both stress constraints (for these loads) and aeroelasticity constraints is performed using the first level model. Loads for the optimized elastic structure are then recalculated again, and a new optimization is carried out. The results found using the first-level model can be used for determination of extreme load cases for the structural parts, along with their corresponding load distribution, determination stiffness requirements and preliminary structural sizing of the lifting surface structure.

The load cases for the full-scale EuRAM airplane were chosen according to prototype data and the results of parametric load and stress analysis in the ARGON computational first and second level models. The primary structure of

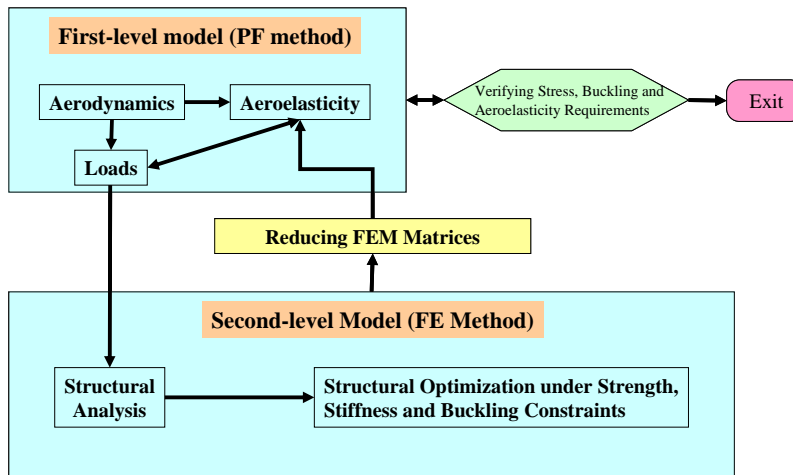


Figure 22: Flow diagram of ARGON system.

V km/h EAS	Mach number	Dynamic pressure kPa	Altitude m
$V_D=690$	$M_D=0.90$	$q_D=22.5$	7400
$V_C=600$	$M_C=0.84$	$q_C=17.0$	8400
$V_A=450$	$M_A=0.37$	$q_A=9.57$	0

Table 1: Design parameters

the wing was considered for flight load cases to study the AWTC characteristics. The following design speeds, Mach numbers and altitudes were chosen (Table1).

The design weight for the load analysis was chosen to equal 215 tons, including 80% mass of the fuel. As a result of parametric flight load analysis, the following design load cases (LC: A, C, D) had been determined: 1) Maximum lift coefficient and maximum load factor at MA, qA near ground; 2) Maximum load factor at MC , qC; 3) Maximum load factor at MD , qD; 4) Half of maximum load factor at MC , qC and deflection of the wing control surfaces to provide roll rate of 10 degrees per second. The fixed and free parameters of trim analysis are shown in Table 2.

The load cases 1-3 were the same for different AWTC configurations. The LC 4 is modified for TA and UWA configurations: parameters TA and UWA are used instead of AILERON. Ensuring the strength under quasi-steady loads for these cases leads to a material distribution which is close to results of recalculations of DSM stiffness according to similarity scale coefficients. For example, Fig. 23 shows displacements and stresses under loads (LC 4) for the basic configuration. An application of these load cases for the wing structural optimization under strength and aeroelasticity constraints for different AWTC configurations was considered in [10] using ARGON second level (FE) model.

The full-scale airplane models with different types and location of AWTC are presented in Fig. 24, where the following abbreviations are used:

- BL - baseline airplane with basic aileron,
- BLP - baseline airplane with winglets,
- TA - airplane with wing tip aileron,
- TAP - airplane with wing tip aileron plus winglets,
- UWA - airplane with under wing aileron,
- UWAP - airplane with under wing aileron plus winglets.

Initially, the structural optimization of the wing-box with stress constraints

LC N.	Fixed Trim parameters	Free Trim parameters
1	$n_z = 2.5, \omega_y = 0, \dot{\omega}_y = 0$	$\alpha, \delta_{Elevator}$
2	$n_z = 2.5, \omega_y \neq 0, \dot{\omega}_y = 0$	$\alpha, \delta_{Elevator}$
3	$n_z = 2.5, \omega_y \neq 0, \dot{\omega}_y = 0$	$\alpha, \delta_{Elevator}$
4	$n_z = 1.25, \omega_x = 10deg/s, \omega_y = 0, \dot{\omega}_y = 0$	$\alpha, \delta_{Elevator}, \delta_{Aileron}$

Table 2: Parameters of trim analysis

Figure 23: Displacements and stresses under loads (LC 4) for basic configuration.

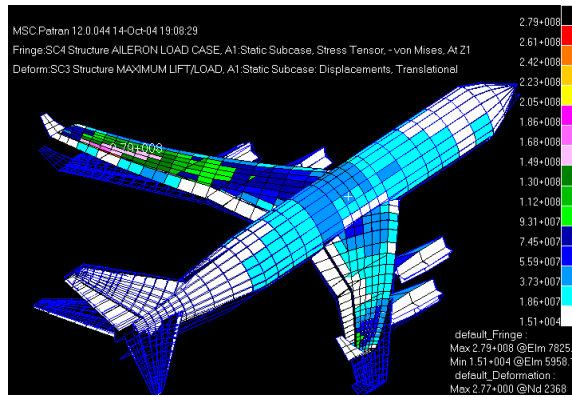
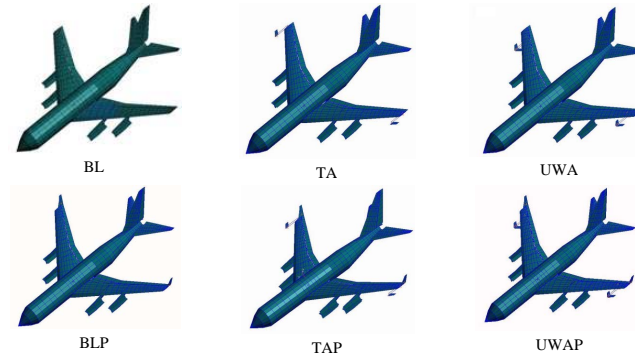


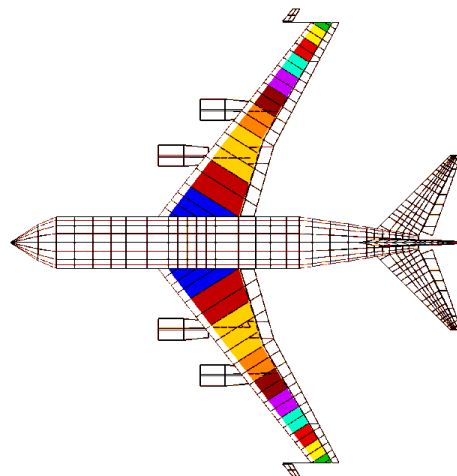
Figure 24: Finite element models of different EuRAM configurations.



was carried out for all configurations under loads obtained without taking into consideration the structural elasticity. The location of the design variables is shown in Fig. 25 using different colors. Ten design variables included the skin thickness, areas of rod elements modeling stringers and areas of spars caps. The proportion between skin thickness and areas of rod elements was defined from the panel buckling constraints and was kept constant throughout the optimization process.

Figure 26 shows the distribution of skin thicknesses along the wing span. It can be seen that for the airplanes with the AWTC, the skin thicknesses are slightly greater than for the baseline airplanes in the root and middle parts of wing. Moreover, the skin thicknesses in the tip part of the wings with AWTC are significantly higher than for the baseline configurations. Therefore, from the viewpoint of strength constraints the baseline configurations are preferable.

Figure 25: Design variables of structural optimization.



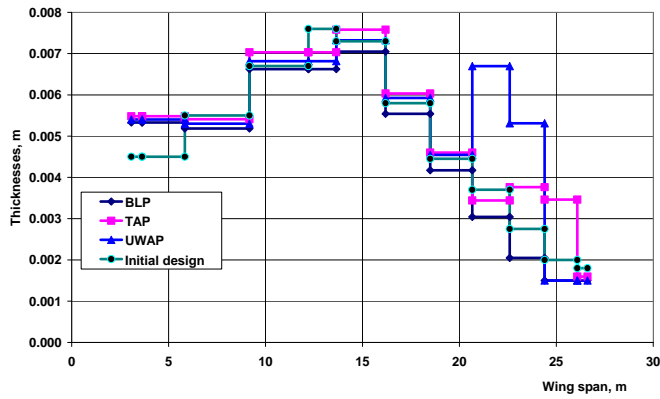


Figure 26: Design variables of structural optimization.

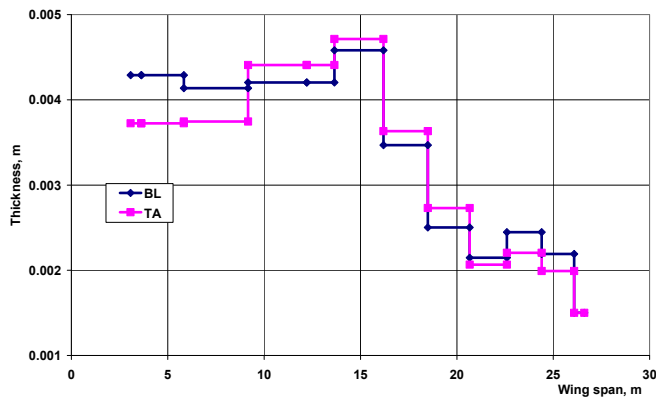


Figure 27: Skin thicknesses stress/aeroelastic optimization.

The analyses of static aeroelasticity characteristics had shown that there is an aileron reversal of the baseline configuration, whereas the EuRAM with the AWTC has sufficient effectiveness in roll. Obviously, the optimized baseline configuration under loads that accounts for structural elasticity has smaller thicknesses and aileron reversal takes place. The optimization of the airplane with the tip aileron (TA) was carried by imposing only stress constraints for the loads on the elastic structure. The optimum weight of the wing panels of structure is about 30% less than the optimum one with "rigid" loads. Aeroelastic analysis showed that the tip aileron effectiveness is sufficient for the considered flight regimes. Structural optimization with stress constraint and aileron effectiveness constraint was then performed for the baseline configuration without winglets under the loads on the elastic structure. The weight was only about 8% less than for the case of "rigid" loads. Such a small decrease of the weight (in comparison with 30% for the airplane with TA) is due to an additional increase of thicknesses in root and tip of the wing to compensate for the violation of the aeroelastic constraints. The distribution of thicknesses for two configurations is shown in Fig. 27. In total, the weight of the wing with AWTC is slightly (about 4%) less than the weight of the wing with regular ailerons. An additional advantage of AWTC is that the control surfaces located forward from the wing leading edge can be used to reduce the manoeuvre loads using their adaptive deflection (when the wing tip aileron is deflected proportionally to the airplane angle of attack).

6. All-Movable Vertical Tail concept

The objective of the concept was to develop and validate novel approaches for increasing the effectiveness of vertical tail surface through the use of an adaptive attachment. All-movable vertical tails are a known design feature [11]. They

Table 3: Vertical tail geometric parameters

	VT	AMVT
Root chord c_0 and c_{0a} [m]	0.900	0.74
Span [m]	1.00	0.80
χ_0 [degs]	46.86	38.0
Tip chord c_1 and c_{1a} [m]	0.250	0.19
C_{MAC-VT} and $C_{MAC-AMVT}$	0.636	0.52
X(25% MAC)	0.59	0.59

were already used in the early days of supersonic flight. For example, they were used on famous airplanes such as the XB-70 and SR-71. Today, the upper part of the vertical tail (VT) on the F-117 is all-movable. An advantage of the adaptive attachment stiffness concept for all-movable tail surfaces is that the size of the tail surface can be reduced by a factor corresponding to the chosen aeroelastic effectiveness increase. The same design failure criteria with respect to flutter can be applied as on conventional designs.

6.1 Geometry and aeroelastic characteristics of basic VT and AMVT

Finite Element models of the traditional vertical tail with rudder, new all-movable fin and of the complete EuRAM airplane were created for multidisciplinary optimization and analysis. In addition to the FE models (in NASTRAN format), the domestic TsAGI software ARGON was used for the design and optimization of the shape and attachment stiffness of AMVT. The main design requirements were defined as follows.

- area of AMVT equals to 65% area of basic VT
- the same position of 25% MAC point for basic VT and AMVT in X direction
- the same aspect ratio
- the same profiles

Minimization of the AMVT structural weight, and accordingly decrease of its stiffness properties, have been restricted by flutter safety requirements in the considered range of rotational stiffness. A structural optimization procedure was performed taking into account the aeroelasticity constraints by using ARGON code in order to determine the geometry and stiffness parameters of AMVT [12]. The photo of the two vertical tails are shown in Fig. 28. Geometric parameters are compared in Table 3.

6.2 Comparison between analysis and experimental results

The aerodynamic side force was computed for an elastic VT, which was connected to the fixed point through rotational springs of different stiffness. The side force increases due to rotational stiffness for axis positions greater than 30% C_{mac} and slightly decreases due to the VT's own elasticity at high speeds (Fig. 29). Figure 30 shows the required stiffness for 1.5 of side force efficiency.

Comparative flutter characteristics of isolated AMVT and complete model with AMVT are shown in Figs 31 and 32. Anti-symmetrical oscillations of the complete DSM change their behavior in the airflow in the presence of adaptive attached AMVT. Dependence of divergence on the flutter speeds on AMVT rotational stiffness, G , are presented for rotational axis position of 40% MAC. Two additional flutter modes have appeared in the case of the complete airplane model. Low-frequency flutter mode "AMVT rotation + rigid body yaw" appears for the complete EuRAM DSM ("Flutter 0.3-1.0 Hz") instead of divergence for isolated AMVT at low rotational stiffness. Due to interaction of rotational oscillations of AMVT with second antisymmetrical wing bending mode and



Figure 28: Comparisons between the two EuRAM vertical tails.

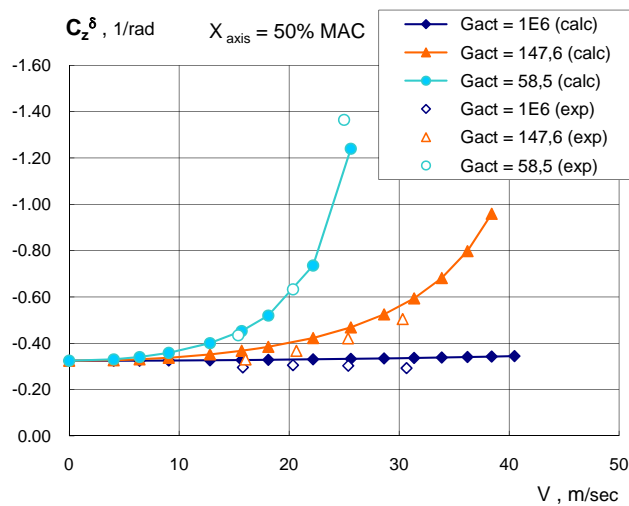


Figure 29: Effectiveness of AMVT in side force for different values of rotational stiffness.

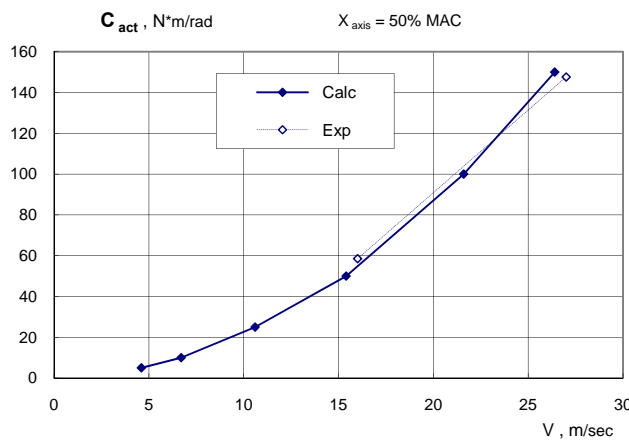


Figure 30: Experimental and calculated results of requirements for the rotational stiffness to provide the side force efficiency of 1.5.

Figure 31: Flutter and divergence of isolated AMVT (left) and of complete AMVT (right).

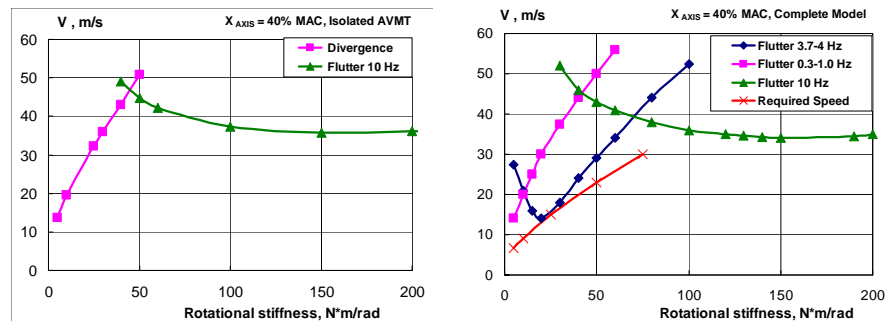
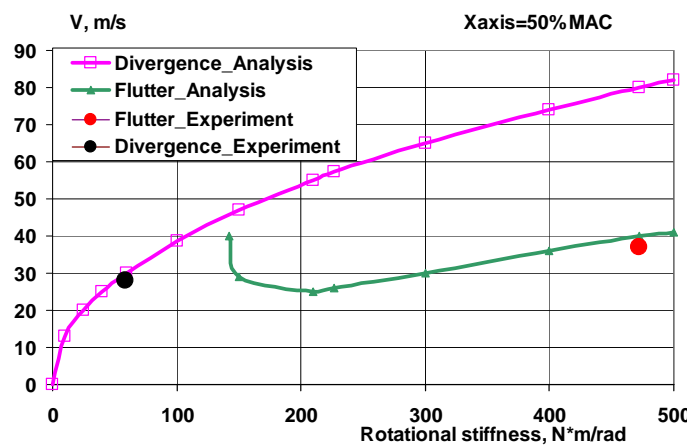


Figure 32: AMVT divergence and flutter speeds vs. rotational stiffness.



fuselage horizontal bending, a new flutter mode ("Flutter 3.7-4.0 Hz", Figure 41) appeared. Figure 31 also illustrates the required flow speed versus rotational stiffness for which side stability and controllability is increased by 1.5 times. It can be seen that the flutter margin is not sufficient for stiffness in the range of 20-30 Nm/rad. An augmentation of flutter margin can be reached by use of active damping in the AMVT actuator. Comparisons of the numerical and experimental results are represented in Fig. 32.

7. Selective Deformable Structure Concept

The objective of the new passive structural design concept is to develop and investigate a slotless connection using "smart" elements of selective deformable structure [13, 14] that allows large continuous deformations of a load-carrying structure. A flexible connection of the aileron leading edge with the wing box was designed for the dynamically scaled model EuRAM. In addition to the ordinary (regular) inner aileron the adaptive aileron was designed (Fig. 33). The static aeroelasticity properties of the adaptive aileron were studied experimentally and theoretically. The main attention was given to behaviour of the wing, where the adaptive aileron has been connected.

7.1 Wind tunnel test

Wind tunnel tests of the EuRAM wing model with the adaptive and ordinary inner aileron were performed in TsAGI subsonic wind tunnel T-103. The adaptive aileron was fabricated using the SDS technology. Figure 34 shows the EuRAM wing with inner and outer ailerons, and with T 103 equipment (external strain gage balance of the wing).



Figure 33: Adaptive aileron.

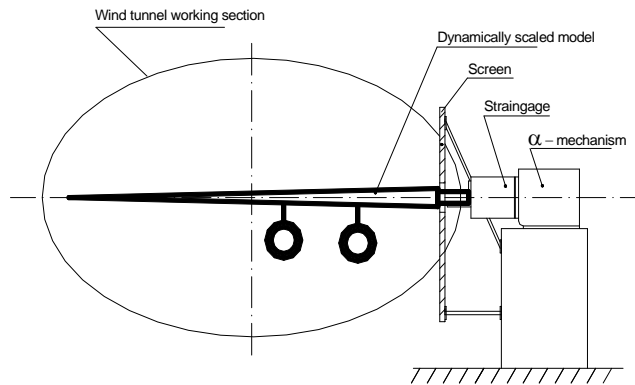


Figure 34: Schematic of the EuRAM wing in T-103.

7.2 Comparison between experimental and theoretical results

Calculated and measured values of rolling moment due to deflection of the ordinary inner and outer ailerons are presented in Fig. 35 (top). The main advantage of using an adaptive aileron structure is the increase of control effectiveness. Lift coefficient derivative with respect to control deflection for wing compartment with adaptive aileron is about 20% higher than for wing compartment with regular aileron. This leads to a better lift to drag ratio, which is about 15% higher than for wing compartment with regular aileron. Fig. 35 (bottom) shows comparisons between experimental lift to drag ratio of the wing compartment with regular and adaptive inner ailerons.

8. Conclusions

Wide multifunctional possibilities and reliability of the EuRAM have been demonstrated during the 3AS project studies. A comprehensive experimental database has been collected. A lot of computational and experimental comparative investigations were performed. They show a good agreement between analytical and test results for different characteristics of strength, stiffness, static aeroelasticity, flutter, aeroservoelasticity, gust loads, etc. Results of the two-level approach for structural optimization of the EuRAM wing under stress and aeroelastic constraints are presented. It was demonstrated that the constraints on aileron effectiveness play a significant role in design of the wing structure. The weight of the wing with AWTC is about 4% less than the weight of the wing with regular ailerons. It was also shown that using of non-traditional wing tip ailerons reduces the weight increase. An all-movable vertical tail (AMVT) with the area equal to 65% area of basic VT was studied. Computation and WT tests showed that AMVT can provide the same yaw stability and control characteristics as basic VT due to elastic adaptive attachment. A slotless connection of the adaptive aileron using "smart" element of Selective Deformable Structures was also investigated. It was demonstrated that lift-to-drag ratio

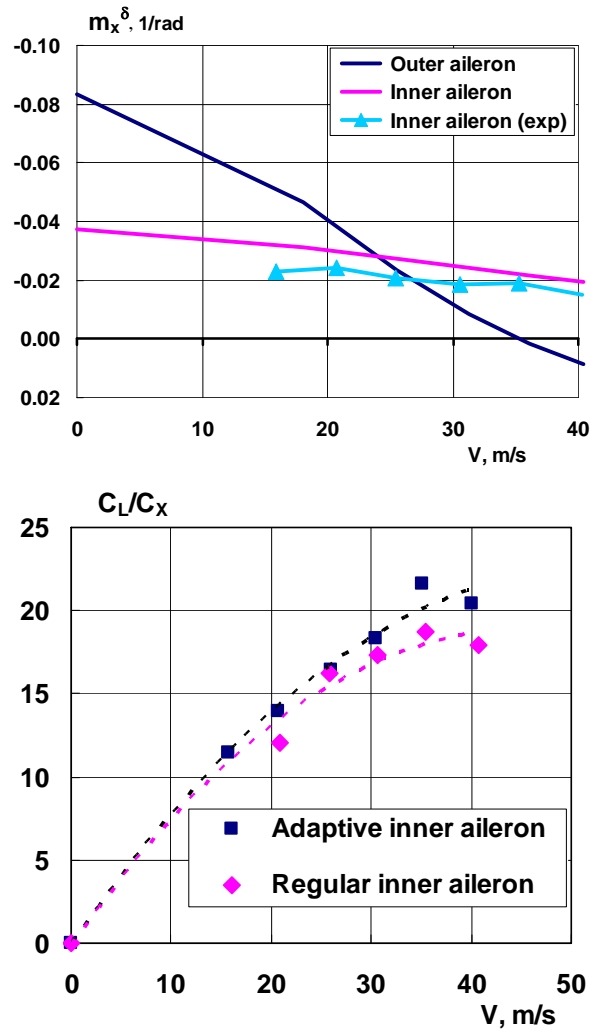


Figure 35: Rolling moment coefficient of EuRAM wing (top) and Lift to drag ratio of EuRAM wing compartment (bottom).

for wing compartment with adaptive aileron is about 15% higher than for wing compartment with regular aileron. The EuRAM has good potential for use in future projects in aeroelasticity.

Acknowledgements

The work was done under financial support in the framework of the 5th FP EC Project "Active Aeroelastic Aircraft Structures (3AS)" and ISTC Grant N.2050. Authors thank project partners for the opportunity for fulfillment of interesting researches and attentive discussion of obtained results.

References

- [1] S. Kuzmina, G. Amiryants, J. Schweiger, J. Cooper, M. Amprikidis, and O. Sensburg. Review and outlook on active and passive aeroelastic design concepts for future aircraft. In *23rd Congress ICAS, Toronto, Canada, 2002*.
- [2] J. Simpson, A. Suleman, and J. Cooper. Review of european research project "active aeroelastic aircraft structures". In *IFASD Conference, Munich, 2005*.

- [3] G.A. Amiryants, M.Ch. Zichenkov, Yu.M. Mullov, and S.V. Shalaev. Design, manufacture and wind tunnel testing of the multi-functional european research aeroelastic model (euram). In *EUCASS Conference, Moscow*, 2005.
- [4] J. Cherdle, V. Chedrik, J. Malecek, and Yu. Naiko. Analysis and experimental validation of an aeroelastic semi-wing model. In *EUCASS Conference, Moscow*, 2005.
- [5] S. Ameduri, M. Amprikidis, J. Cooper, and J. San Millan. Adaptive stiffness system for an active aeroelastic all-moving vertical tail. In *EUCASS Conference, Moscow*, 2005.
- [6] F. Ishmuratov and V. Chedrik. Argon code: Structural aeroelastic analysis and optimization. In *IFASD Conference, Amsterdam*, 2003.
- [7] V. Chedrik, F. Ishmuratov, and S. Kuzmina. Numerical studies of aeroelasticity/strength/ aerodynamic for the european research aeroelastic model. In *EUCASS Conference, Moscow*, 2005.
- [8] A.B. Kudryashov, F.Z. Ishmuratov, V. Chedrik, S. Kuzmina, and J. Schweiger. Main aspects of fe modelling and active aeroelasticity concept analysis of the passenger aircraft (euram). In *Symposium: Aviation Technologies of the XXI Century (ASTEK-03), Zhukovsky, Russia*, 2003.
- [9] M. Karpel and B. Moulin. Gust loads alleviation using special control surfaces. In *IFASD Conference, Munich*, 2005.
- [10] S. Kuzmina, V. Chedrik, and F.Z. Ishmuratov. Strength and aeroelastic structural optimization of aircraft lifting surfaces using two-level approach. In *6th World Congress of Structural and Multidisciplinary Optimization, Rio de Janeiro, Brazil*, 2005.
- [11] J. Schweiger, F. Weiss, and Th. Kullrich. Active aeroelastic design of a vertical tail for a fighter aircraft. In *8th AIAA/NASA/ISSMO Symposium on Multidisciplinary Analysis and Optimization, CP-4848, Long Beach, CA*, 2000.
- [12] S. Kuzmina, F. Ishmuratov, M. Zichenkov, V. Kuzmin, and J. Schweiger. Integrated numerical and experimental investigations of the active adaptive all-movable vertical tail concept. In *IFASD Conference, Munich*, 2005.
- [13] G. Amiryants. Selectively deformable structures; new concept in engineering. In *ICAS Conference, Melbourne*, 1998.
- [14] G. Kawiecki and G. Amiryants. Adaptive selectively deformable structures analysis. In *IFASD Conference, Amsterdam*, 2003.